chemengineering

Supplementary Materials

Nomenclature	
f	Fugacity, mol m^{-3}
G	Gibbs free energy, J mol^{-1}
N_{ij}	Number of moles of component i in reaction j
R_{const}	Ideal gas constant, J K^{-1} mol^{-1}
T	Temperature, K
Greek symbols	
μ_i	Chemical potential of component i, J mol^{-1}
Superscript	
o	Standard state

1. Scanning electron microscopy–Energy dense X-Ray spectroscopy of the $Cu/ZnO/Al_2O_3$ catalyst

SEM-EDS results confirmed the presence of Cu, Zn, Al and O in the catalyst. The SEM micrograph (Figure S1a) shows a catalyst consisting of a large number of isolated and agglomerated globular catalyst particles. The EDS maps (Figure S1b) show a very homogeneous distribution of Cu, Zn and Al in the catalyst, which is expected to result in beneficial interactions between well-mixed and uniformly spread nanoparticles, especially Cu and ZnO.

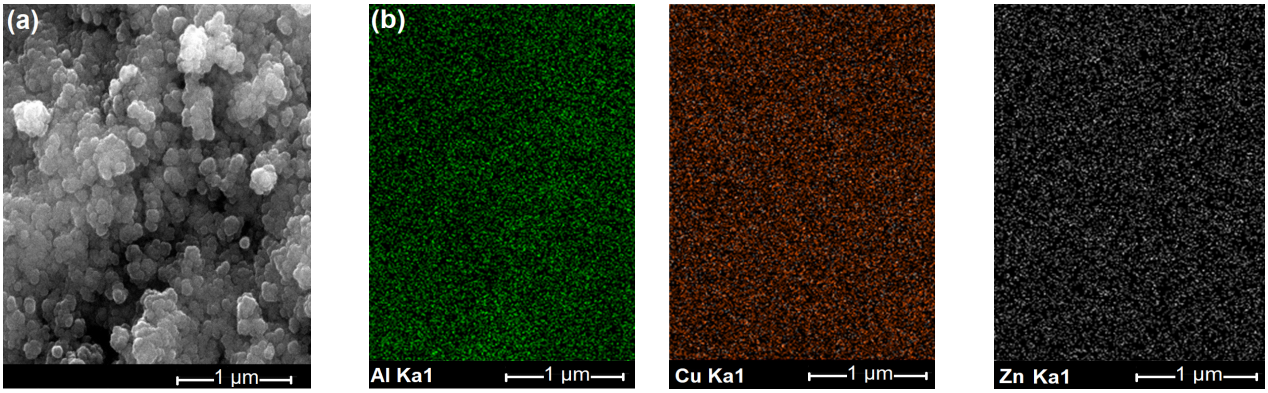

Figure S1. Commercial $Cu/ZnO/Al_2O_3$ catalyst: (a) morphology displayed on the SEM micrograph and (b) EDS maps of elemental distribution: Al (green), Cu (red) and Zn (black).

2. N_2 adsorption/desorption profile of the $Cu/ZnO/Al_2O_3$ catalyst

The N_2 adsorption/desorption profile of the catalyst corresponds to a Type IV isotherm with a H1 hysteresis loop, which is a characteristic of catalysts with a mesoporous structure [48].

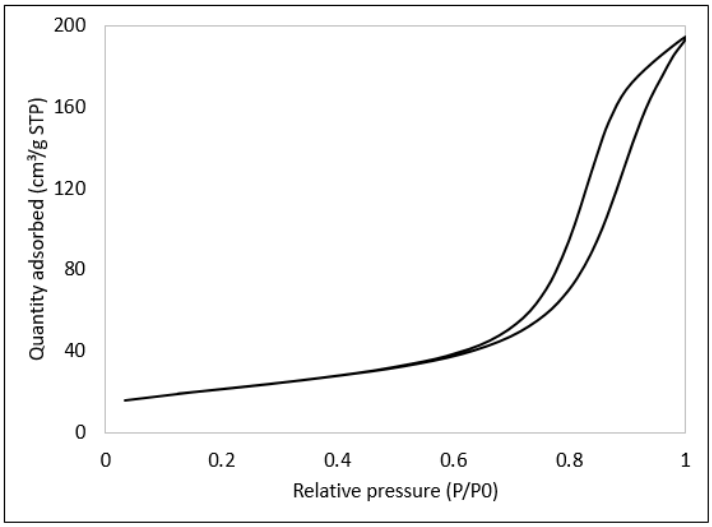

Figure S2. Isothermal (–196 °C) linear plot of the N_2 adsorption/desorption on the Cu/ZnO/Al_2O_3 catalyst.

3. X-ray diffractogram of the Cu/ZnO/Al_2O_3 catalyst

The XRD diffractogram of the catalyst (Fig S3) confirmed the presence of CuO and ZnO. Al_2O_3 peaks were not visible, probably because of their low content or amorphous nature.

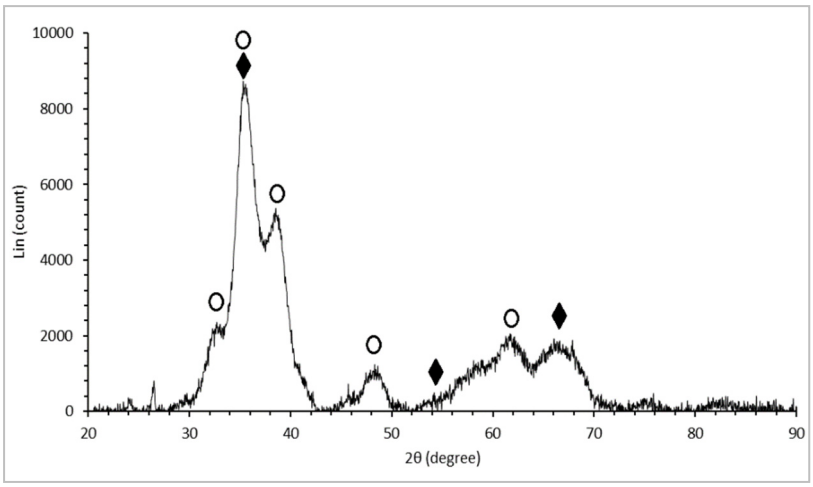

Figure S3. XRD diffractogram of the Cu/ZnO/Al_2O_3 catalyst showing typical CuO (♦) and ZnO (○) peak positions as reported in the literature [14,18,39].

4. Transmission electron microscopy of the Cu/ZnO/Al_2O_3 catalyst

The TEM micrographs (Fig. S4) reveal that the catalyst components (Cu, ZnO and Al_2O_3) are hardly distinguishable. Furthermore, the fact that the particles are not well shaped can also denote a low level of crystallinity of the catalyst components [9], TEM micrographs suggest an intimate contact between Cu and ZnO particles. This has been reported to enhance the catalytic performance of Cu/ZnO/Al_2O_3 [9,14].

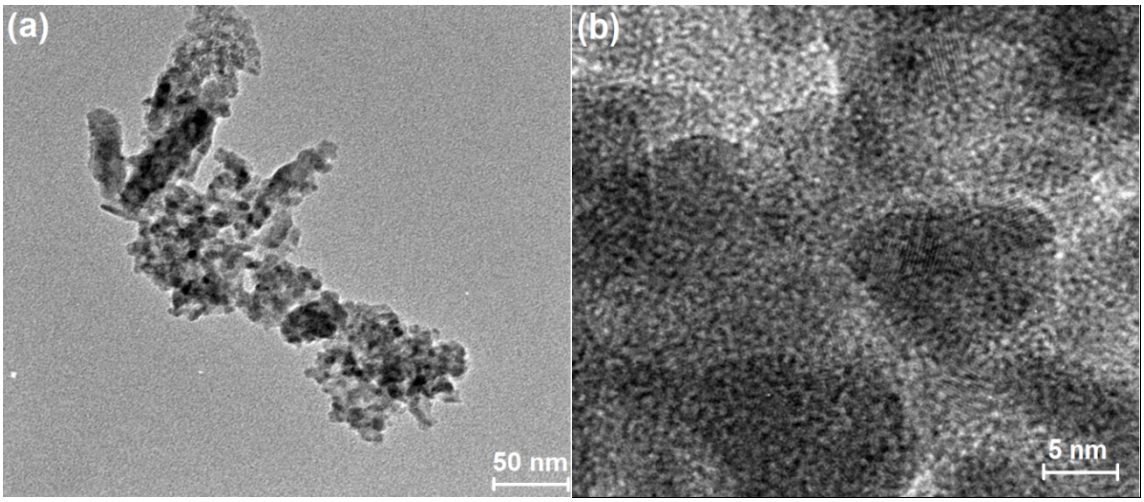

Figure S4. $Cu/ZnO/Al_2O_3$ catalyst: (a) low-magnification and (b) high-magnification TEM micrographs.

5. Catalyst temperature programmed reduction profile

H_2 temperature programmed reduction profile (Fig. S5) was used for the determination of the $Cu/ZnO/Al_2O_3$ catalyst reduction temperature. A reduction temperature of 230 °C was used in the reduction of the catalyst prior to experiments.

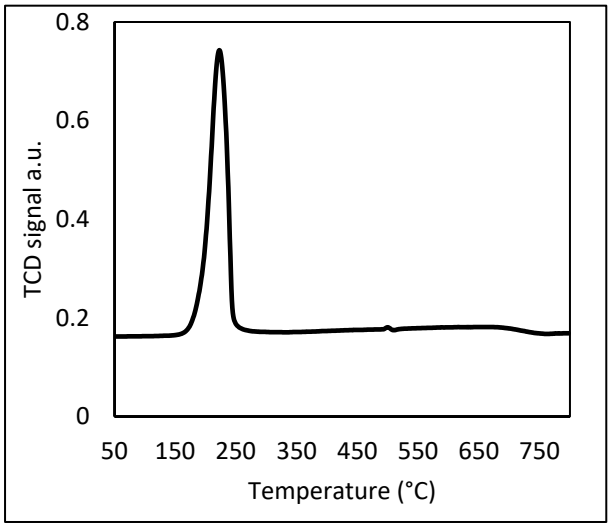

Figure S5. H_2-TPR profile of the $Cu/ZnO/Al_2O_3$ catalyst.

6. Equilibrium calculations

Equilibrium calculations were performed using ASPEN v8.6 Gibbs equilibrium reactor (RGibbs). In order to simulate the direct CO_2-to-MeOH process, and generate the equilibrium CO_2 conversion and methanol selectivity curves, the feed composition was set to 75% H_2 and 25% CO_2, and the products were set to include CO, H_2O, the unreacted CO_2 and H_2. The RGibbs works on the principle of Gibbs free energy minimisation, which is a non-stoichiometric method, assuming that a system of n components involved in r reactions is thermodynamically favoured when the change in Gibbs dG free energy is minimum [49,50].

$dG = \sum_{i=1}^{n} \sum_{j=1}^{r} \mu_i \, dN_{ij} = 0.$

In Eq. B1, the chemical potential μ_i of component i is calculated by

$$\mu_i = R_{const}\, T \left[G_i^0 + \ln\left(\frac{f_i}{f_i^o}\right)\right].$$

Neither methane nor other hydrocarbons were part of the product gas. Hence, the CO_2 hydrogenation to MeOH and reverse water gas shift were the only possible reactions in the system.